Control of Surface Configuration by Application of Concentrated Loads

David Bushnell*
Lockheed Palo Alto Research Laboratory, Palo Alto, Calif.

The literature on active control of mirrors is briefly reviewed. An analysis method is formulated in which the surface quality of free axisymmetric spherical mirrors is controlled by actuators that produce concentrated forces or self-equilibrating moment pairs. Normal displacement fields arising from unit actuator loads are generated with the use of thin shell theory by discretization of the radial coordinate and trigonometric expansion of the circumferential coordinate. It is found that local ripples caused by rather closely spaced self-equilibrating moment actuators are more pronounced than those caused by single force actuators, indicating that the former are not as suitable for surface quality control as the latter.

Introduction

Problem Definition

CURRENTLY there is much interest in the possibility of orbiting large diameter telescopes and antennas. One of the major problems to be solved involves the design, fabrication, and maintenance of a telescope primary mirror 1 m or more in diameter, the surface of which must be controlled to a root mean square (rms) tolerance of about 10^{-8} m. Similarly, the parabolic surface of a microwave antenna of the order of 100 m in diameter must be maintained to a tolerance of less than 1 mm. Factors that make those close tolerances extremely difficult to achieve include: continuously changing thermal gradients; the necessity of constructing and testing the structure in a gravitational environment for operation at zero g; initial fabrication imperfections due to uneven polishing, residual stresses, or imperfect mandrels; random vibrations generated by spacecraft operation; and possible constraints on the design from the requirement that the spacecraft deploy automatically.

In order to correct an initially imperfect large surface area and maintain it to the tolerances just mentioned, it is necessary to control it "actively" by means of actuators in response to a changing environment. This problem involves the following elements: 1) initial design of the structure, the surface of which is to be accurately controlled; 2) prediction of the response of this structure to known disturbances; 3) decision as to what type of actuators to use to control the surface (e.g., force, moment, or displacement actuators); 4) decision as to the number and locations of the actuators; 5) decision as to the type, number, and location of surface sensors; and 6) decision as to what control law to use and its implementation.

State-of-the-Art

In the past decade, especially from 1969-1973, much new knowledge was accumulated as a result of NASA's Large Space Telescope (LST) program on how to design, build, and control a large primary mirror.[1] In particular, several papers were written[2-8] on the "active mirror" or "active optics" concept—a concept in which the mirror surface contour is changed and controlled continuously in time by actuators on its rear surface. Crane,[2] in work begun in 1966, reports on the design and construction of a 20-in.-diam, three-segment mirror, a wavefront sensing system, and a control system for maintaining the surface quality to within 1/20 of a wavelength of light. In Crane's system each segment moved as a rigid body. Ryabova[3] reviews this and other work on the concept of active optical control by means of multiple rigid mirror segments.

In a series of papers, each adding to the results of the last, Creedon and Robertson,[4] Robertson,[5] Creedon and Lindgren,[6] Howell and Creedon,[7] and Ostroff[8] discuss the control of a deformable single-segment primary spherical mirror by means of actuators which apply normal forces to the rear surface. They fabricated a glass mirror with a 0.762-m diam 1.27-cm thickness, and 4.52 m radius of curvature. Applying normal forces with 60 equally spaced actuators, they reduced an initial rms error in the surface figure from $>1/2$ to $<1/50$ of a wavelength of light. In Refs. 6-8 the initial distortions of the mirror are expressed as a series of vibration modes, and a subset of these modes is controlled. The modes are derived in a closed form for a flat plate in Ref. 6 and numerically by means of computer programs[9,10] for a shell in Ref. 7. Howell and Creedon[7] describe a technique for selecting the actuator locations: the actuators are placed near common nodal lines of uncontrolled modes. Ostroff[8] refines this technique in an automated computer program by selecting actuator locations on the basis of minimizing that part of the energy which is in the uncontrolled (but known) modes and selecting sensor locations to minimize the energy of the unobserved (but known) modes.

A similar body of knowledge was generated in the years 1973-1977 by investigators who are interested in actively controlling a smaller initially flat optical surface in order to compensate for phase distortions and divergence of optical beams propagating in a turbulent and absorbing atmosphere. Hayes et al.,[11] and Pearson et al.[12] describe multisegment approaches, while Crawford et al.,[13] Primmerman and Fouche,[14] Neufeld,[15] Hardy et al.,[16] and Pearson and Hansen[17] describe deformable mirror systems. Presumably because the mirrors involved in these studies are generally smaller than those involved in the Large Space Telescope program, and because the characteristic times involved in counteracting atmospheric turbulence are many orders of magnitude shorter than the orbital frequency that governs the time variation of the thermal distortion of the telescope primary mirror, the experiments described in Refs. 14 and 17 included piezoelectric or displacement actuation rather than force actuation of the mirror surface. The use of displacement rather than force actuators considerably raises the natural frequency spectrum of a mirror. ("Displacement actuator" implies a device that is stiff compared to the structure being controlled; the control system generates displacement commands. "Force actuator" implies a device with a soft spring; the control system generates force commands.) Hardy[18] has recently published an excellent survey paper on active optical systems.

Received July 7, 1977; revision received Aug. 24, 1978.

Index category: Structural Design.

*Staff Scientist. Associate Fellow AIAA.

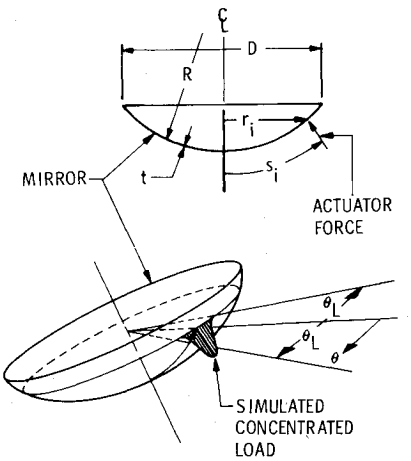

Fig. 1 Spherical mirror with simulated concentrated load, $V_i(\theta)=[1+\cos(\pi\theta/\theta_L)]/(2r_i\theta_L)$ for $-\theta_L\le\theta\le\theta_L$; $V_i(\theta)=0$ for $|\theta|>\theta_L$.

This Paper

In the previous work on this subject, the emphasis has been on control system design and analysis. The mirrors, while curved in some cases, had rather low diameter-to-thickness ratios ($D/t=100$ in Ref. 4, 60 in Ref. 5, and 80 in Ref. 17).

If the mirrors were not flat, they were so shallow relative to thickness that they behaved essentially as flat plates. In this paper the emphasis is on the static analysis of axisymmetric curved mirrors, behaving as thin shells as they deform due to concentrated actuator loads. Dynamics and control theory lie beyond the scope of this treatment. The aim here is to describe an efficient analysis method for the study of active control of surfaces and to give the reader a physical feeling for the behavior of axisymmetric curved shells subjected to concentrated actuator forces and moments. The problem of controlling the surface configuration of nonuniformly heated mirrors is addressed in a following paper.[19]

Analysis

The Model

The mirror is assumed to be an axisymmetric spherical shell segment, as shown in Fig. 1. The wall construction may be monocoque or layered, isotropic or orthotropic. This spherical segment may be initially deformed by some nonuniform temperature distribution which varies around the circumference and through the thickness or by some arbitrarily prescribed initial nonsymmetric normal displacement distribution, such as a measured imperfection.

Force or moment actuators are modeled in this analysis as concentrated loads. These concentrated loads are represented analytically as nonuniform line loads distributed around the circumference, as shown in Figs. 1 and 2. One force actuator is represented as a single load acting normal to the shell surface at a given meridional station $s=s_i$. In the circumferential direction this load is distributed as

$$f(\theta)=[1+\cos(\pi\theta/\theta_L)]/2 \qquad -\theta_L\le\theta\le\theta_L$$

$$f(\theta)=0 \qquad |\theta|>\theta_L \tag{1}$$

The load/(circumferential arc length) that, when integrated over the range $-\theta_L\le\theta\le\theta_L$, yields a unit load is

$$V_i(\theta)=f(\theta)/(r_i\theta_L) \tag{2}$$

The results obtained here and in Ref. 19 are based on $\theta_L=5$ deg. One self-equilibrating moment actuator, an example of which is depicted in Fig. 3, is represented as two equal and opposite line moments, each distributed around the circumference as shown in Fig. 2 and acting at two distinct meridional stations, denoted A and B in Fig. 3.

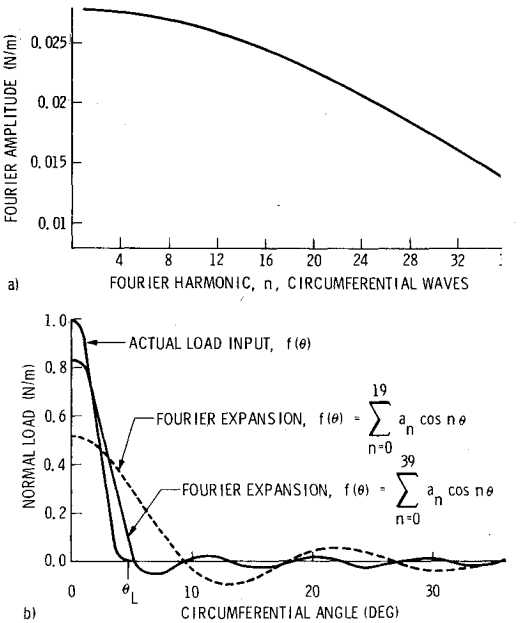

Fig. 2 Convergence of line load $f(\theta)$ with increasing number of circumferential harmonics: a) Fourier coefficients, a_n; b) Load input $f(\theta)$ for $\theta_L=5$ deg and two finite Fourier series representations of $f(\theta)$.

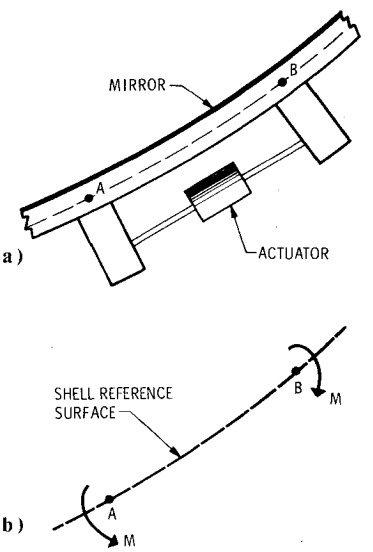

Fig. 3 a) Moment actuator and b) BOSOR6 model.

The fact that the concentrated force or moments are spread out in the circumferential direction can be best justified physically on the grounds that in an actual design each actuator would most likely act against a nonstructural pad that would serve to distribute the point load over a finite length of circumference. The representation of an actuator by a load is valid provided that the actuator spring constant is small compared to the effective stiffness of the shell against which the actuator is pushing.

The Fourier cosine series for $f(\theta)$ converges very slowly, as seen in Fig. 2a. In the limit of vanishingly small θ_L, the series does not converge at all. The coefficient of every term except that corresponding to $n=0$ approaches the vanishingly small constant θ_L/π. However, the response of the structure to each circumferential harmonic of the concentrated load does converge reasonably fast, as shown in Fig. 9, which will be discussed again in a following section. Therefore, the results obtained here and in Ref. 19 are not strongly dependent on θ_L for $\theta_L\le 5$ deg. For example, from Fig. 9 it is seen that for a

force actuator at the edge of a certain mirror 4 m in diameter, the load harmonic in Fig. 2a corresponding to $n=20$ contributes about 4.5×10^{-8} m of normal displacement at the actuator. If θ_L had been taken as zero, this contribution would have been about $(.0277/.023)\times4.5\times10^{-8}$ m or 5.42×10^{-8} m. Thus, for true concentrated loads, the curves in Fig. 9 would be very slightly less downward sloping than they now are. The most important low harmonics would not be significantly affected.

Finding Actuator Forces Required to Minimize rms Surface Error

The objective of the analysis is, for a given initial distortion and a given number and distribution of actuators (concentrated loads), to find the magnitudes of the the actuator forces or moments that compensate for this initial distortion such that the mean-squared surface configuration error E^* is minimized. (E^* will be defined in a following equation). Let the initial distortion $e(s,\theta)$, normal to the mirror surface, be given by

$$e(s,\theta)=\sum_{n=0}^{nmax} g_n(s)\cos n\theta+\sum_{n=1}^{nmax} h_n(s)\sin n\theta \tag{3}$$

The normal displacement field $d(s,\theta)$ caused by N actuators (see Fig. 4) is

$$d(s,\theta)=\sum_{i=1}^{N+3} a_i\sum_{n=0}^{nmax} f_{in}(s)\cos n(\theta-\theta_i) \tag{4}$$

The mirror is assumed to be free floating. Hence, without some constraint, the displacement field due to a single non-self-equilibrating actuator force would be indeterminate because of possible rigid body motion. This problem is solved by choice of a meridional station at which to prevent axial and circumferential displacements corresponding to the $n=0$ and $n=1$ circumferential harmonics of the Fourier series representation of the concentrated load. In the BOSOR6 analysis this constraint can be applied at any radial station. Since the rigid body components are removed from the influence functions, $f_{in}(s)$ $i=1, N$, it is necessary to reintroduce them as additional influence functions. Not doing this would be equivalent to using an incomplete set of functions to represent an arbitrary mirror displacement field. Consequently, the mean-squared surface configuration error E^* would be overestimated.

The three terms in Eq. (4) corresponding to $N+1$, $N+2$, and $N+3$ are rigid body modes

$$a_{N+1}\sum_{n=0}^{nmax}\delta_n^0\left(1-\frac{s^2}{2R^2}\right)\cos n(\theta-0)+a_{N+2}\sum_{n=0}^{nmax}\delta_n^1 r\cos n(\theta-0)$$
$$+a_{N+3}\sum_{n=0}^{nmax}\delta_n^1 r\cos n(\theta-\pi/2) \tag{5}$$

in which the δ_n^k, $k=0$ or 1, are Kronecker deltas. The coefficient a_{N+1} represents rigid body axial displacement; a_{N+2} represents either tilt about the $\theta=90$ deg axis or translation parallel to the $\theta=0$ deg axis, and a_{N+3} represents either tilt about the $\theta=0$ deg axis or translation parallel to the $\theta=90$ deg axis. An influence function corresponding to rotation about the axis of revolution is not introduced because it does not contain any displacement component normal to the mirror surface and hence does not contribute to the surface error.

The mean-squared surface configuration error E^* is defined as

$$E^*(a_1,a_2,\ldots a_{N+3})=\frac{1}{\text{Area}}\int_\theta\int_s(d+e)^2 r\,ds\,d\theta \tag{6}$$

Minimization of E^* with respect to the actuator forces, a_i, $i=1,\ldots N$ and rigid body motion components a_i, $i=N+1$, $N+2$, $N+3$ leads to a system of $N+3$ linear simultaneous equations

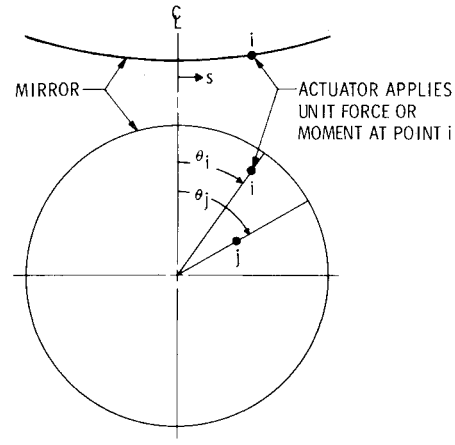

Fig. 4 Free mirror with actuator at point *i*. Deflection at *j* due to a unit actuator load at *i* is:

$$d_j=\sum_{n=0}^{nmax} f_{in}(s_j)\cos n(\theta_j-\theta_i)$$

$$A\bar{a}=\bar{F} \tag{7}$$

in which $\bar{a}$ is the vector containing the actuator force amplitudes and rigid body displacement component amplitudes.

Since the structure is free to move as a rigid body, it is necessary to introduce three constraint conditions in the solution of Eq. (7). The three constraint conditions, introduced by the Lagrange multiplier method, are:

$$\lambda_1\sum_{i=1}^{N} a_i\cos\varphi_i=0 \tag{8a}$$

$$\lambda_2\sum_{i=1}^{N} a_i\sin\theta_i(r_i\cos\varphi_i+z_i\sin\varphi_i)=0 \tag{8b}$$

$$\lambda_3\sum_{i=1}^{N} a_i\cos\theta_i(r_i\cos\varphi_i+z_i\sin\varphi_i)=0 \tag{8c}$$

in which $\lambda_1,\lambda_2,\lambda_3$ are the Lagrange multipliers; φ_i is the polar angle to the ith actuator; and z_i is the axial distance from the mirror pole to the point s_i at which the actuator force is applied. Equation (8a) corresponds to equilibrium of axial forces; Eq. (8b) corresponds to equilibrium of moments about the $\theta=0$ deg axis; and Eq. (8c) corresponds to equilibrium of moments about the $\theta=90$ deg axis.

It can be shown that the (i,k)th element of the matrix A is given by

$$A_{ik}=\pi\sum_{n=1}^{nmax}\left[\int_s f_{in}(s)f_{kn}(s)r\,ds\,\cos n(\theta_i-\theta_k)\right]$$
$$+2\pi\int_s f_{i0}(s)f_{k0}(s)r\,ds \tag{9}$$

and the ith element of the vector $\bar{F}$ is given by

$$F_i=-\pi\sum_{n=1}^{nmax}\int_s g_n(s)f_{in}(s)r\,ds\,\cos n\theta_i$$
$$-2\pi\int_s g_0(s)f_{i0}(s)r\,ds-\pi\sum_{n=1}^{nmax}\int_s h_n(s)f_{in}(s)r\,ds\,\sin n\theta_i \tag{10}$$

The integrations over meridional arc length s are performed numerically, since the functions f, g, and h are defined only at

discrete nodal points, as will be discussed in the next section. The mean-squared error E^* can be computed from Eq. (6) once Eq. (7) has been used to calculate the a_i, $i=1,2,...N+3$. The root-mean-squared (rms) surface error ratio, a measure of surface quality, is defined as

$$E=\left[E^*\Big/\left\{\frac{1}{\text{Area}}\int_\theta\int_s e^2 r\,ds\,d\theta\right\}\right]^{1/2} \tag{11}$$

Calculation of Unit Load Influence Functions and Static Response to an External Disturbance

The linear static response of the axisymmetric shell to nonuniform temperature or to a unit concentrated load acting anywhere on its surface is determined from a computer program BOSOR6 for the analysis of axisymmetric structures.[20] This program is based on a direct-stiffness finite-difference method analogous to the finite-element method.[21] In BOSOR6 the independent variables, meridional arc length s, and circumferential coordinate θ are separated. Thus, the displacement field $q(s,\theta)$ is expressed in the form:

$$q(s,\theta)=\begin{Bmatrix}u(s,\theta)\\ v(s,\theta)\\ w(s,\theta)\end{Bmatrix}=\begin{Bmatrix}\sum_{n=0}^{n\max} u_{n1}(s)\cos n\theta+\sum_{n=1}^{n\max} u_{n2}(s)\sin n\theta\\ \sum_{n=1}^{n\max} v_{n1}(s)\sin n\theta+\sum_{n=0}^{n\max} v_{n2}(s)\cos n\theta\\ \sum_{n=0}^{n\max} w_{n1}(s)\cos n\theta+\sum_{n=1}^{n\max} w_{n2}(s)\sin n\theta\end{Bmatrix} \tag{12}$$

in which u,v, and w are the meridional, circumferential, and normal displacement components, respectively. The meridional coordinate s is discretized, and a set of simultaneous linear algebraic equilibrium equations for each circumferential harmonic n

$$\boldsymbol{K}_n\bar{q}_n=\bar{Q}_n \tag{13}$$

is derived by minimization of the energy functional with respect to the nodal point displacement components. In Eq. (13) the vector $\bar{q}_n$ contains the discrete nodal point displacement components u_n, v_n, and w_n along a meridian and Lagrange multipliers for constraint conditions, if any. Since the discretization is in one coordinate only, the stiffness matrix $\boldsymbol{K}_n$ has a very small bandwidth ($=7$). Hence, for each circumferential wavenumber n, the system of equations (13) can be set up and solved with a very small expenditure of computer time.

Unit Load Influence Functions

The BOSOR6 computer program is first used in a series of linear analyses to find J times $n$max static deflection fields $q_{jn1}(s)$ of a shell or plate subjected to a unit concentrated load acting at $\theta=0$ and at a series of meridional stations s_j. The subscript "1" denotes the summations with u_{n1}, v_{n1}, w_{n1} in Eq. (12). Note that the second summations on the right-hand sides of Eqs. (12) are not needed for calculation of the influence functions $f_{in}(s)$ because the function $f(\theta)$ in Eq. (1) can be represented by a Fourier cosine series. The vector $q_{jn1}(s)$ contains a triad of displacement components $u_{jn1}(s)$, $v_{jn1}(s)$, and $w_{jn1}(s)$ evaluated at each nodal point along the discretized shell meridian. A new condensed vector $f_{jn}(s)$ is formed by retention of only the normal displacement component $w_{jn1}(s)$, since only this component affects the optical quality of the mirror surface. Thus, a two-dimensional set of influence functions, $f_{jn}(s)$, $j=1,2,...J$, $n=0,1,2,...$ $n$max, is derived in J separate executions of BOSOR6. The subscript j indicates the meridional location of the concentrated load (actuator), and the subscript n indicates the Fourier series harmonic. These influence functions are stored for later use by a separate computer program, ACTUATOR, which solves

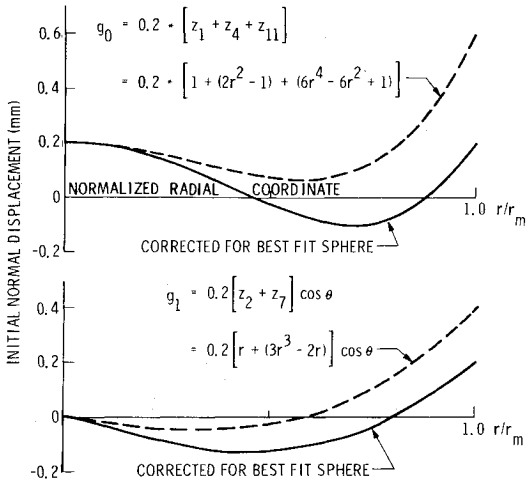

Fig. 5 Initial normal displacement distributions g_0 and g_1 at $\theta=0$ deg before and after removal of the defocus ($n=0$) and tilt ($n=1$) components for the best-fit sphere.

Eq. (7) with constraint conditions (8) by means of an algorithm written by Felippa,[22] calculates E in Eq. (11), and plots the initial and residual error fields over the mirror surface.

The input to BOSOR6 includes the shell geometry, material properties of each layer of the shell wall, and the meridional position of the unit normal force or positions A and B (Fig. 3) of the unit moments.

Static Response to an External Disturbance

Once the influence functions $f_{jn}(s)$ have been calculated and stored, BOSOR6 can be used next to find the initial distortion harmonics $g_n(s)$ and $h_n(s)$ $n=1,2,...n$max [Eq. (3)] if these arise from some physically identifiable source such as nonuniform heating or gravity. Note that unless the external disturbance has at least one plane of symmetry, the second summations on the right-hand sides of Eqs. (12) will be nonzero. The input to BOSOR6 for this analysis includes the temperature distribution and/or body forces and support reactions. The resulting functions $g_n(s)$ and $h_n(s)$ are then stored for later use by the program ACTUATOR. If it is desired to prescribe an initial distortion rather than derive one from BOSOR6, the program ACTUATOR can be used to compute the Fourier harmonics $g_n(s)$ and $h_n(s)$ given some arbitrarily specified normal displacement matrix $w(s,\theta)$.

Modification of Initial Distortion Field for "Best Fit" Sphere

Certain components of the initial distortion $g_n(s)$ and $h_n(s)$ of the primary mirror correspond only to a change in the position of the focus and therefore need not be removed by actuators but may instead be counteracted by appropriate displacement and rotation of a secondary mirror. These include $n=0$ and $n=1$ rigid body components and an $n=0$ component equivalent to a uniform change in the mirror radius of curvature. For example, if a flat circular mirror is heated uniformly over its surface but has temperature varying linearly through the thickness, it will deform into a shallow spherical shape. The only component of this displacement that must be removed by actuators is the deviation of this very shallow spherical shape from a best-fit parabola, which would be a very small percentage of the total distortion. (In the analysis reported here, the perfect mirror profile is assumed to be spherical rather than parabolic, so that in this example no correction by primary mirror actuation would take place.)

If the shell is shallow, the $n=0$ components of the normal displacement w that would require no correction by actuators are given by

$$w_0(s)=w_{\text{axial}}(1-0.5s^2/R^2)+0.5(1/R-1/R_1)s^2 \tag{14}$$

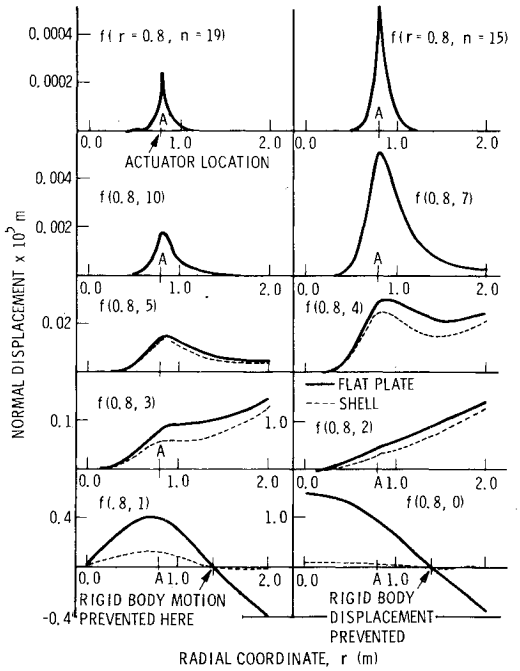

Fig. 6 Influence functions for curved and flat mirrors produced by a unit force at $r = 0.8$ m.

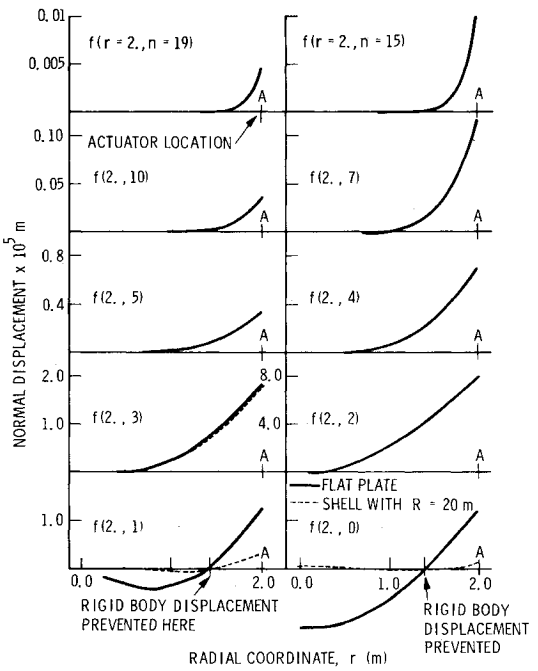

Fig. 7 Influence functions for curved and flat mirrors produced by a unit force at the edge, $r = 2$ m.

in which the first term arises from a rigid body axial displacement w_{axial} and the second term arises from a uniform change in mirror curvature, $(1/R - 1/R_1)$. In the ACTUATOR program the quantities w_{axial} and $1/R_1$ are determined by minimization of

$$\int_\theta \int_s [w_0(s) + g_0(s)]^2 r\,ds\,d\theta \tag{15}$$

with respect to w_{axial} and $1/R_1$. The distribution $w_0(s)$ is then subtracted from $g_0(s)$ and the new $n = 0$ distortion field, $g_0(s) - w_0(s)$, is used in Eq. (10) instead of $g_0(s)$. Modification of $g_1(s)$ and $h_1(s)$ for tilt about $\theta = 90$ deg and 0 deg, respectively, is handled in the same way. In this case the

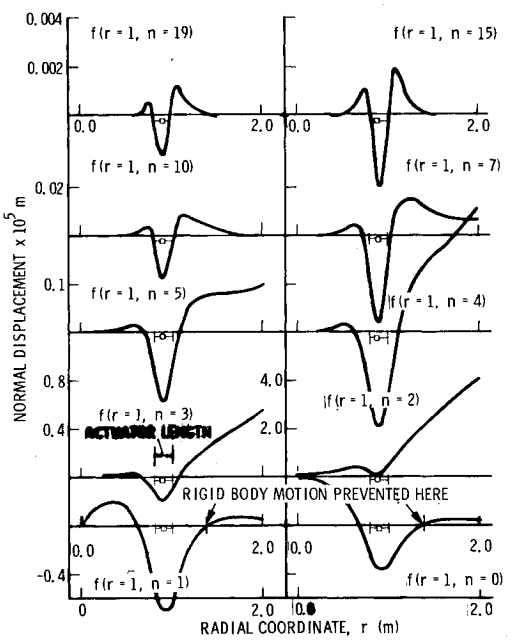

Fig. 8 Influence functions for curved mirror produced by a unit self-equilibrating moment pair at $r_A = 0.8$ m and $r_B = 1.0$ m.

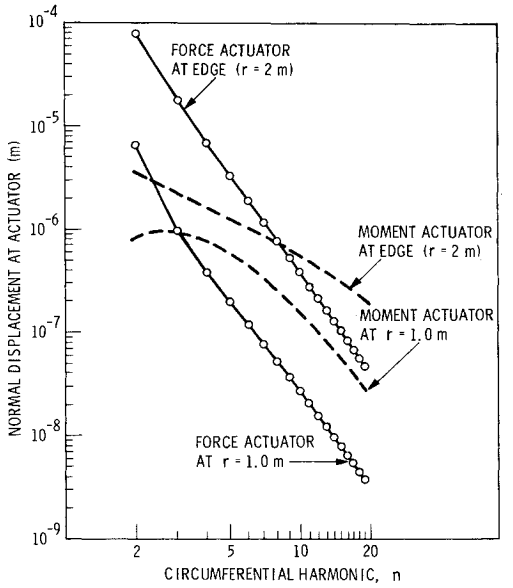

Fig. 9 Maximum normal displacement near actuator vs n for unit actuator loads on curved mirror with radius of curvature $R = 20$ m.

$n = 1$ components of the normal displacement w that would require no correction by actuators are given by

$$w_1 = a_1 r\cos\theta + a_2 r\sin\theta \tag{16}$$

and a_1 and a_2 are determined by minimization of

$$\int_\theta \int_s [w_1 + g_1(s) + h_1(s)]^2 r\,ds\,d\theta \tag{17}$$

with respect to a_1 and a_2. An example of modification of the $n = 0$ and $n = 1$ initial distortion harmonics of the best-fit sphere is shown in Fig. 5. The Z_i in Fig. 5 are Zernike polynomials[23] in the radial coordinate r.

Numerical Results

The method just described has been used to investigate the behavior of various actively controlled mirrors. In this section influence functions corresponding to force and self-

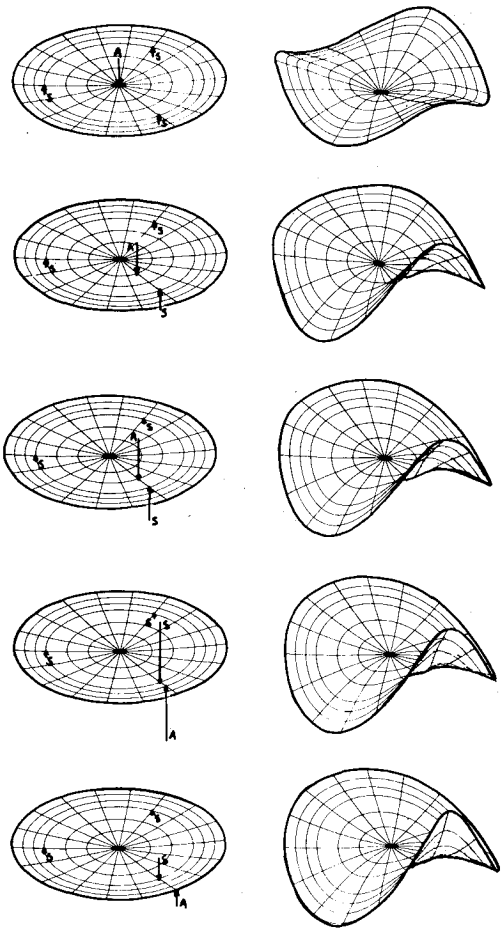

Fig. 10 Deformations of 1-cm-thick, 4-m diam sandwich spherical mirror supported at three points S and with one active force actuator A located at various radii r_A.

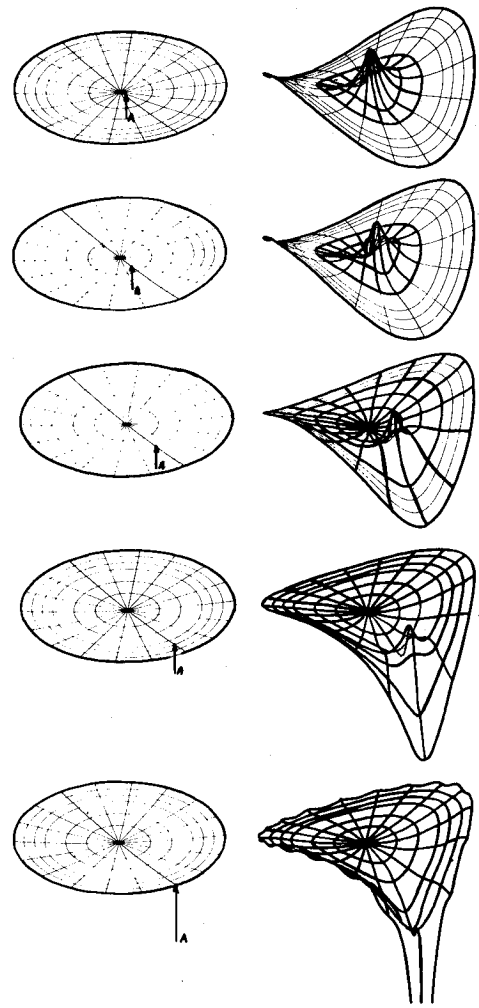

Fig. 11 Deformations of the spherical cap with one self-equilibrating moment pair located at varous radii r.

equilibrating moment actuators acting on a mirror with sandwich wall construction are plotted. Results from BOSOR6 are compared with a test performed by Creedon and Robertson in 1969.[4] In Ref. 19, rms surface configuration errors are calculated for nonuniformly heated sandwich and monocoque mirrors before and after application of actuator loads. The rms residual surface error is plotted there as a function of the number, location and type of actuators.

Why Sandwich Wall Construction?

A sandwich wall construction is advantageous because of its high bending stiffness to weight and bending stiffness to extensional stiffness ratios. Skogh[24] has found that for hemispherical shells with sandwich wall construction of total thickness t, the decay length associated with self-equilibrating bending discontinuity stresses is the same as that for a monocoque shell of thickness $\sqrt{3}t$. This property, which arises from the high bending to extensional stiffness ratio of the sandwich wall, is helpful in the case of a mirror loaded by actuators because the amplitudes of local ripples produced on the mirror surface by concentrated loads with given spacing are less than they would be for a monocoque shell of the same thickness.

Influence Functions

Figures 6 and 7 show influence functions corresponding to force actuators acting on a plate and a shell. Both the plate and the shell have diameters of 4 m and are 1-cm thick with sandwich wall construction. The face sheets of the sandwich are 1-mm thick, with modulus $E=6.74\times10^{10}$ N/m^2 and Poisson's ratio $\nu=0.3$. The core modulus is 6.74×10^3 N/m^2. The radius of curvature of the shell is $R=20$ m. From Figs. 6 and 7 it is seen that the spherical shell behaves significantly differently from a circular plate only for circumferential harmonics n less than about 4. The large differences for $n=0$ and $n=1$ arise from the fact that the plate deforms inextensionally in these harmonics but the spherical shell does not. Thus, much of the potential energy of the $n=0$ and $n=1$ harmonics of the applied concentrated load creates membrane strain energy in the shell which is associated with small out-of-plane distortions.

Figure 8 depicts influence functions of a self-equilibrating moment actuator located on the shell as shown in the figure. Note that the influence functions exhibit more reversals in slope than do those for the force actuators shown in Figs. 6 and 7. These meridional "ripples" cause difficulties, as described next and in Ref. 19.

Figure 9 reveals an interesting fact: The rate of decrease with increasing n of normal displacement created by self-equilibrating moment actuators is slower than that created by force actuators. As seen in Fig. 8, self-equilibrating moment actuators, the length of which is small compared to the mirror diameter, cause local ripples in the mirror surface of larger amplitude than those caused by force actuators. (However, Scott[25] found that long moment actuators are quite effective for controlling the surface quality of flat mirrors.)

Figures 10 and 11 show isometric views of mirrors deformed by one active actuator located at five different radii. The lengths of the arrows indicate the magnitudes of the actuator (A) and (in Fig. 10) support (S) forces. The supports are located at 120 deg intervals at $r=0.69r_{max}$. In Fig. 11 the arrow indicates the location of the point B in Fig. 3. The other end of the moment actuator is at $r_A=r_B-0.2$ m. Only

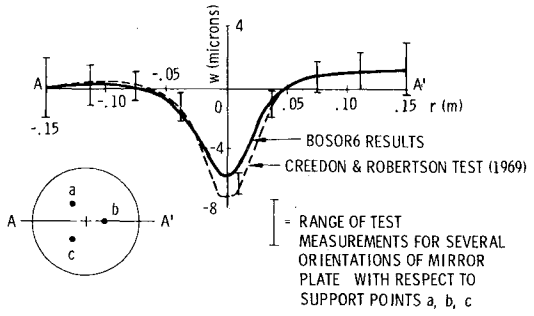

Fig. 12 Comparison of BOSOR6 results with test by Creedon and Robertson (1969).

Fig. 11 (self-equilibrating moment actuator) shows the influence functions $f_{in}(s)\cos n\theta$ of Eq. (4), although the amplitude scale vaies from the top of Fig. 11 to the bottom. In Fig. 10 (force actuator) the deformation pattern is complitude scale varies from the top of Fig. 11 to the bottom. In course dependent on the circumferential coordinate of the active actuator. Comparison of Figs. 10 and 11 shows that self-equilibrating moment pairs corresponding to the rather short actuator shown in Fig. 8 cause greater localized surface deflections than do single force actuators, indicating that the former are not as suitable for surface quality control as the latter.

Comparison With Test

Figure 12 shows a comparison between the BOSOR6 analysis and a test by Creedon and Robertson.[4] The glass spherical mirror has diameter of 30.5 cm, thickness of 0.317 cm, and radius of curvature of 152 cm, and is loaded by a force actuator at the center and supported at 3 points, a,b,c at $r=3.81$ cm. The plot corresponds to the diameter AA'. The curves have been shifted axially so that w at point A is zero. The considerable scatter of test results for different orientations of the mirror with respect to the support points a,b, and c probably arises from circumferentially varying mirror thickness, material properties, and initial mirror shape.

Conclusions

An advantage of the analysis method described here is that it is efficient on the computer. Influence functions need be calculated only as a function of actuator radial location. Computation of the influence functions requires only short computer times because the bandwidth of the stiffness matrix $\boldsymbol{K}_n$ in Eq. (13) is very small. Convergence studies are easily performed because the analytical model involves discretization only in the radial coordinate direction.

The flow of computations is arranged such that influence functions corresponding to various radial locations of a single actuator are first calculated and stored on a disk or drum file. This need be done only once for each design choice. Root-mean-squared residual surface error can then be calculated for different external disturbances and distributions of actuators. Results of such parameter studies are presented in Ref. 19.

Acknowledgments

This research was sponsored by the Lockheed Independent Research and Independent Development Programs. The author is grateful for the many helpful conversations with and suggestions of D. Aspinwall and J. Skogh during the course of this work.

References

[1] Workshop Proceedings, *Optical Telescope Proceedings*, NASA SP-233, May 1969.

[2] Crane, R., Jr., "An Experimental Twenty-Inch Segmented Active Mirror," *IEEE Transactions on Aerospace and Electronics Systems*, AES-5, 1969, pp. 279-286.

[3] Ryabova, N. V., "Sectional Active Mirrors for Telescopes," *Soviet Journal of Optical Technology*, Vol. 42, 1975, pp. 675-687.

[4] Creedon, J. F. and Robertson, H. J., "Evaluation of Multipoint Interaction in the Design of a Thin Diffraction-Limited Active Mirror," *IEEE Transactions on Aerospace and Electronic Systems*, AES-5, 1969, pp. 287-293.

[5] Robertson, H. J., "Development of an Active Optics Concept Using a Thin Deformable Mirror," NASA CR-1593, Aug. 1970.

[6] Creedon, J. F. and Lindgren, A. G., "Control of the Optical Surface of a Thin, Deformable Primary Mirror with Application to an Orbiting Astronomical Observatory," *Automatica*, Vol. 6, 1970, pp. 643-660.

[7] Howell, W. E. and Creedon, J. F., "A Technique for Designing Active Control Systems for Astronomical Telescope Mirrors," NASA TN D-7090, Jan. 1973.

[8] Ostroff, A. J., "Evaluation of Control Laws and Actuator Locations for Control Systems Applicable to Deformable Astronomical Telescope Mirrors," NASA TN D-7276, Oct. 1973.

[9] Melosh, R. J. and Christiansen, H., "Structural Analysis and Matrix Interpretive System (SAMIS) Program," NASA TM 33-311, Nov. 1966.

[10] MacNeal, R. M., *The NASTRAN Theoretical Manual*, NASA SP-221, 1970.

[11] Hayes, C. L., Brandewie, R. A., Davis, W. C., Mevers, G. E., and Soohoo, J., "Coherent Optical Adaptive Techniques (COAT)," Rockwell International, Anaheim, Calif., Report C72-731/501, Feb. 1973.

[12] Pearson, J. E., Bridges, W. B., Hansen, S., Nussmeier, T., and Pedinoff, M. E., "Coherent Optical Adaptive Techniques: Design and Performance of an 18-Element Visible Multidither COAT System," *Applied Optics*, Vol. 15, 1976, pp. 611-621.

[13] Crawford, F. S., Schwemin, A. J., Smits, R. G., Muller, R. A., and Buffington, A., "Active Image Restoration with a Flexible Mirror," Berkeley Lawrence Radiation Lab. Rept. No. CONF-750645-2, June 1975.

[14] Primmerman, C. A. and Fouche, D. G., "Thermal Blooming Compensation: Experimental Observations Using a Deformable Mirror System," *Applied Optics*, Vol. 15, 1976, pp. 990-995.

[15] Neufeld, C., "Modal Wavefront Control System (MOWACS)," Perkin Elmer Corp., Norwalk, Conn., Rept. PE-13039, July 1976.

[16] Hardy, J. W., Lefebvre, J. E., and Koliopoulos, C. L., "Real Time Atmospheric Compensation," *Journal of the Optical Society of America*, Vol. 67, 1977, pp. 360-369.

[17] Pearson, J. E. and Hansen, S., "Experimental Studies of a Deformable-Mirror Adaptive Optical System," *Journal of Optical Society of America*, Vol. 67, 1977, pp. 325-333.

[18] Hardy, J. W., "Active Optics: A New Technology for the Control of Light," *Proceedings of the IEEE*, Vol. 66, June 1978, pp. 651-697.

[19] Bushnell, D., "Control of Surface Configuration of Nonuniformly Heated Shells," *AIAA Journal*, Vol. 12, Jan. 1979, pp. 78-84.

[20] Bushnell, D., "Stress, Buckling, and Vibration of Hybrid Bodies of Revolution," *Proceedings of AIAA/ASME/SAE 17th Structures, Structural Dynamics and Materials Conference*, May 1976, pp. 16-36; also *Computers and Structures*, Vol. 6, 1976, pp. 221-239.

[21] Bushnell, D., "Finite-Difference Energy Models Versus Finite Element Models: Two Variational Approaches in One Computer Program," *Numerical and Computer Methods in Structural Mechanics*, Academic Press, New York and London, 1973, pp. 291-336.

[22] Felippa, C. A., "Solution of Linear Equations with Skyline-Stored Symmetric Matrix," *Computers and Structures*, Vol. 5, 1975, pp. 13-29.

[23] Born, M. and Wolf, E., *Principles of Optics*, Second ed., Pergamon Press, New York, 1959, p. 465.

[24] Skogh, J., "Analysis of Hemispherical Cap for Lockheed Aircraft Services," unpublished report, Lockheed Missiles and Space Co., Palo Alto, Calif., Oct. 1964.

[25] Scott, R. M., "New Technique for Controlled Optical Mirror Shapes," *Optical Engineering*, Vol. 14, 1975, pp. 112-115.